SMATCH BENCHMARK: SEISMIC RESPONSE ANALYSIS OF THE BASE-ISOLATED CRUAS NPP SUBJECTED TO LE-TEIL EARTHQUAKE USING THE REAL-ESSI SOFTWARE

Constantinos Kanellopoulos[1], Bozidar Stojadinovic[2], Sara Ghadimi Khasraghy[3], and Tadeusz Szczesiak[4]

[1] PhD Candidate, ETH Zurich, Switzerland (kanellopoulos@ibk.baug.ethz.ch)
[2] Professor, ETH Zurich, Switzerland (stojadinovic@ibk.baug.ethz.ch)
[3] Dr., Swiss Federal Nuclear Safety Inspectorate (ENSI), Switzerland (sara.ghadimi@ensi.ch)
[4] Dr., Swiss Federal Nuclear Safety Inspectorate (ENSI), Switzerland (tadeusz.szczesiak@ensi.ch)

ABSTRACT

This study examines the seismic response of the base-isolated Cruas Nuclear Power Plant (NPP) during the 11.11.2019 Le-Teil earthquake within the international benchmark SMATCH using the finite element (FE) software Real-ESSI. The Cruas NPP is modelled with nine buildings on a continuous upper raft foundation, seismically isolated by laminated steel-neoprene bearings. Seven buildings, including one reactor building, are represented as lumped-mass stick models, while detailed 3D-FE models are used for one reactor and one auxiliary building. The study aims to: (a) blindly predict the seismic response of the Cruas NPP during the Le-Teil earthquake; and (b) calibrate the FE model by comparing simulated accelerations with recorded data at three sensor locations. Linear elasticity with Rayleigh damping is assumed for all structural and soil elements, with the isolators modelled as viscoelastic springs in all three directions. The main FE model used during the blind prediction stage was a Domain Reduction Method (DRM)-based model introducing vertically propagating, three-component seismic waves (S-waves in the two horizontal directions and P-waves vertically) through the provided horizontal soil layer profile matching free-field acceleration records. Another fixed-base model neglecting the Soil-Structure-Interaction (SSI) effects excited at its base with the free-field acceleration records was used for comparison. In the blind prediction case, the fixed-base model either underestimated or overestimated the recorded data but offered overall a better approximation, while the DRM model consistently underestimated the recorded accelerations. Calibrating the isolators' effective horizontal stiffness to account for directional variations in their distortion level and adopting a more representative soil profile around the NPP significantly improved the DRM model's agreement with the recorded data. However, the remaining discrepancies after calibration may suggest that, for this shallow earthquake, the actual earthquake impact is not represented sufficiently by the conventional assumption of vertically incident waves, highlighting the need for careful selection of the DRM model parameters.

INTRODUCTION

On November 11, 2019, a magnitude 4.9 (Mw) earthquake struck approximately 15 km from the Cruas Nuclear Power Plant (NPP), a base-isolated 900 MW Pressurized Water Reactor (PWR) in the lower Rhone Valley, France. Known as the Le-Teil earthquake, it occurred at an exceptionally shallow focal depth of about 1.5 km (Viallet et al., 2022). Thanks to the seismic instrumentation system deployed by EDF, sensors installed at a nearby free-field site and within the main structures of the Cruas NPP successfully recorded the seismic event. To promote knowledge exchange on the seismic design and assessment of base-isolated NPPs, EDF (Électricité de France) and IRSN (Institut de Radioprotection et de Sûreté Nucléaire) organized an international benchmark under the OECD-NEA (Nuclear Energy Agency). The benchmark consists of two phases: the first assesses the accuracy of engineering methods in computing seismic ground motion at the Cruas site, while the second focuses on calculating the seismic response of the base-isolated Cruas NPP. Each phase includes a blind prediction stage, followed by a calibration process using recorded seismic data.

The Swiss Federal Nuclear Safety Inspectorate (ENSI) contributed to the second phase of the SMATCH benchmark by supporting three teams from Basler & Hofmann, Stangenberg & Partners, and ETH Zurich. This paper focuses on the ETH-ENSI team's work, presenting two finite element (FE) models developed to analyze the seismic response of the Cruas NPP. The first model employs the Domain Reduction Method (DRM) (Bielak et al., 2003) to introduce seismic motion into the local soil domain, generating S- and P-waves that produce the prescribed three-component free-field motion at the ground surface. The second model applies the free-field motion directly at the base of a fixed-base NPP model. The FE model descriptions are followed by blind prediction results, comparing the two models against recorded data, and concluding with the calibration of the most consistent model, identified as the first DRM model.

DESCRIPTION OF THE FINITE ELEMENT MODEL

The dynamic time-history analysis of the Cruas NPP subjected to the Le-Teil earthquake was conducted using the Real-ESSI Simulator software (Jeremic et al., 2025). Real-ESSI incorporates the DRM, enabling realistic input of seismic motions into the local soil domain. OpenSees (McKenna et al., 2010) was used exclusively for the eigenvalue analysis of the fixed-base Cruas NPP model. The time-history simulations were performed on the Euler parallel computing cluster, operated by the ETH Zurich High-Performance Computing group, and on a local computer at UC Davis, provided by Professor Jeremic. The open-source mesh generator Gmsh (Geuzaine & Remacle, 2009) was used to generate or re-mesh model parts where needed (e.g., generate soil domain), while ParaView (Ahrens et al., 2005) was used for results visualization.

Figure 1 provides an overview and cross-section of the FE model developed to analyze the seismic response of the Cruas NPP during the Le-Teil earthquake. The provided mesh file includes nine NNP buildings on a continuous upper raft foundation, seismically isolated with laminated steel-neoprene bearings. This study adopts the provided 3D geometry of one reactor and one auxiliary building, while simplified stick models with lumped masses represent the remaining buildings (including the second reactor building). The sensor locations EAU 001, 002, and 003 (Figure 1) correspond to the positions where seismic recordings were obtained, which the FE model aims to reproduce. The NPP buildings are modeled using different element types: (a) Euler-Bernoulli beam elements (black in Figure 1) for the stick models and certain parts of the detailed 3D models, with the provided truss elements replaced by equivalent beams with negligible moment of inertia. Stiff beam elements (turquoise in Figure 1) enforce diaphragm action at floor levels and "rigidly" connect the stick models to their foundation. (b) Linear elastic 4-node shell elements model the detailed 3D reactor and auxiliary buildings, the upper and lower raft foundations, and the perimeter wall. (c) Very stiff linear elastic uniaxial spring elements (white in Figure 1) elevate the reactor building to the correct level, addressing limitations from shell-element modeling of the thick foundation. (d) Lumped mass elements (purple spheres in Figure 1) are assigned to various parts of the reactor and auxiliary buildings, in addition to those of the stick models.

The upper raft foundation of the Cruas NPP is supported by 1812 laminated steel-neoprene bearings (Viallet et al., 2022), placed on reinforced concrete (RC) supports modeled as beams, each accommodating 2, 4, or 8 bearings, and resting on a lower raft foundation. Figure 2 provides an overview of the support positions and seismic isolators (highlighted in yellow ochre). To approximate the nonlinear hysteretic behavior of the rubber bearings in an equivalent-linear manner, three Kelvin-Voigt elements per support are used (see inset of Figure 2), each consisting of a linear spring and a viscous damper connected in parallel. The end nodes of the two horizontal Kelvin-Voigt elements are constrained to the slab node directly above the RC support using master-slave constraints, as illustrated in the inset of Figure 2.

The first five soil layers, extending to 20 m depth, are explicitly modeled using linear elastic 8-node solid elements, based on the provided shear wave velocity profile at the free-field RAN sensor near the NPP

site (see Figure 8). The mesh discretization ensures accurate propagation of shear waves up to 20 Hz. To separate the NPP from the surrounding soil, a perimeter wall of shell elements, connected to the lower raft foundation, is included. These RC shell elements are 1 meter thick, as approximately derived from the cross-sectional view of the NPP shown in Viallet et al. (2022). Bonded contact elements tie the soil to both the foundation and the perimeter wall using the penalty stiffness method.
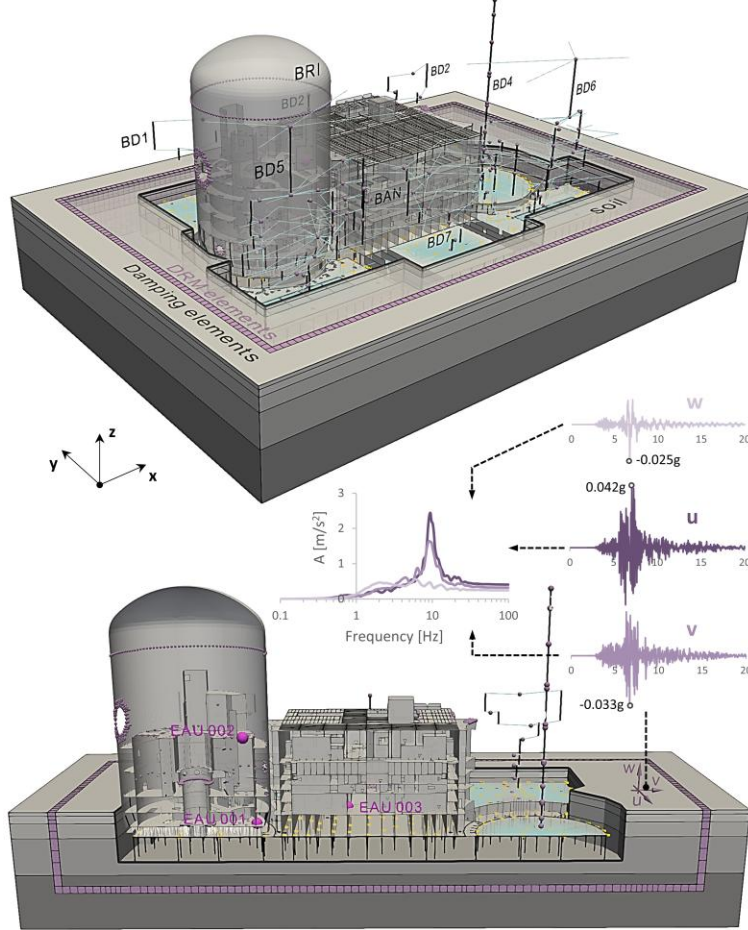

Figure 1. Overview and cross-section of the first 3D DRM FE model of the Cruas NPP. The generated S- and P-waves in the two horizontal and vertical directions, respectively, result in the recorded three-component free-field motion at the ground surface. The sensor locations, EAU 001, 002, and 003, are highlighted in magenta.
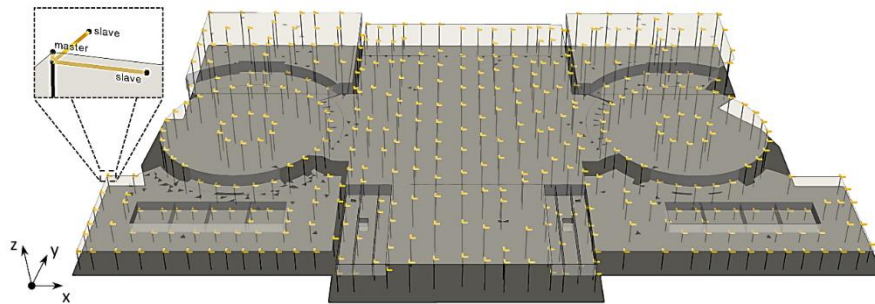

Figure 2. Overview of the isolator locations (highlighted in yellow ochre) positioned between the lower and upper raft foundations. Each support features 2, 4, or 8 isolators, modeled using two horizontal and one vertical Kelvin-Voigt elements (see inset for a detailed view).

The primary dynamic analysis employs the DRM to introduce seismic motion into the model, generating a three-component ground surface motion matching the provided free-field acceleration time histories in the v, u, and w directions (corresponding to the x, -y, and z directions of the FE model, respectively) (Figure 1) recorded by the RAN sensor. With the DRM applied, fixed boundaries are assumed at the lateral and bottom sides of the model. A Rayleigh damping ratio of 2% is assigned to all structural components and 3% to all soil layers of the inner DRM domain. Progressively increasing Rayleigh damping (outwards) is applied to the outer DRM domain (refer to Damping elements in Figure 1). The fixed-base model of the Cruas NPP (i.e., without the soil) is also analyzed using the provided three-component RAN motion, with a 5% Rayleigh damping ratio for its structural components. During the blind prediction stage, results from both analyses are compared to recorded data. In the subsequent calibration stage, only the DRM model is refined, as it was deemed the most consistent among the two models.

PART I – BLIND PREDICTION

Base isolation properties

Each support is assigned three Kelvin-Voigt elements (two horizontal and one vertical) to model the base isolators in the x, y, and z directions, respectively. This requires determining two horizontal stiffness values and one vertical stiffness value, along with their respective damping coefficients. The horizontal stiffness, K_h, for each isolator is calculated as $K_h = (G_d \cdot A)/t_r$, where G_d is the effective dynamic shear modulus of the laminated steel-neoprene bearing (practically dictated by the rubber's properties), A is the sheared rubber area, and t_r is the total rubber thickness (i.e., the sum of the thicknesses of the individual layers). The geometrical properties of the bearings are publicly available (Viallet et al., 2022), with $A = 500^2$ mm^2, and $t_r = 40.5$ mm. To estimate G_d, data from progressive distortion tests conducted in 1980, 1985, 1990, and 2008 (Figure 3) were provided. As aging increases G_d over time, an aging curve was supplied to extrapolate test data to the year of the earthquake (2019), producing the petrol-colored points in Figure 3. Initially, a logarithmic curve (dashed line in petrol) was assumed to fit these points, yielding $G_d \approx 2.6$ MPa at the "Le Teil" distortion level (0.064, as provided by the organizers), which was used to compute K_h. However, due to limited test data at the distortion level of interest, this assumption is likely an oversimplification. Since modal analysis results of the Cruas NPP fixed-base model were provided during the blind prediction stage, it was considered more reliable to calibrate K_h to match the given eigenmodes and eigenfrequencies. Parametric analysis using OpenSees determined that $K_h = 19.6$ MN/m (per isolator
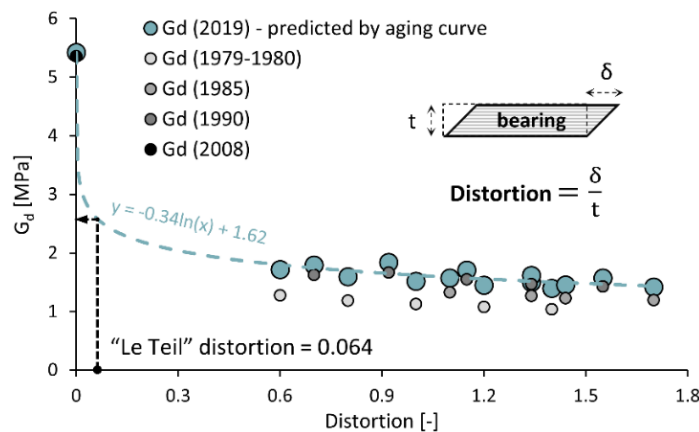

Figure 3. Progressive distortion tests of the laminated steel-neoprene bearings. Effective dynamic shear modulus–distortion ($G_d - Distortion$) response of the isolators tested in 1980, 1985, and 1990 (greyscale points), along with extrapolated values for the year of the earthquake (2019) (petrol points). The fitted dashed logarithmic curve provides a preliminary approximation.

4

in the x and y directions) best reproduced the eigenmodes and eigenfrequencies, as shown in Figure 4. This corresponds to G_d = 3.175 MPa, which was adopted during the blind prediction stage *for both horizontal directions*. The assumption that the isolators exhibit identical effective horizontal stiffness in both directions—despite the strong nonlinearity of G_d at the distortion level of interest—is justified for two reasons. First, the calibration yielded excellent agreement with the provided eigenmodes and eigenfrequencies. Second, the benchmark provided a single "Le-Teil" distortion value (0.064), implying that the distortions in the x and y directions during the earthquake were either identical or very similar—a presumption that would later be proven incorrect.
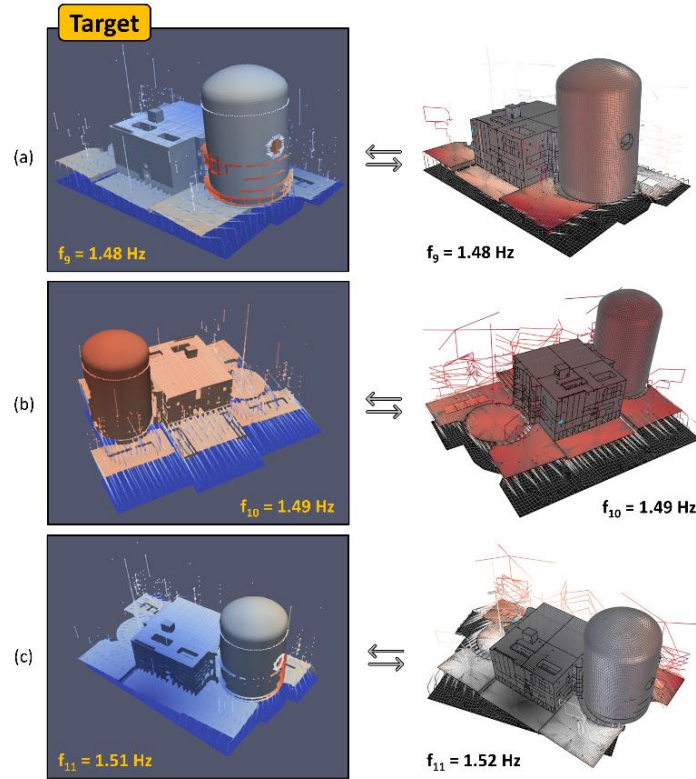

Figure 4. Fundamental eigenmodes and eigenfrequencies of the fixed-base Cruas NPP model. Comparison between the provided results (left) and those calculated in OpenSees (right), used to calibrate the horizontal stiffness of the isolators during the blind prediction phase.

The vertical stiffness, K_v, of the laminated steel-neoprene bearing is determined as $K_v = (E_c \cdot A)/t_r$ where E_c is the effective compression modulus of the steel-rubber composite (calculated for a single rubber layer) under the specified vertical load, A is the axially loaded area of the bearing (A = 490^2 mm^2), and t_r is the total rubber thickness (t_r = 40.5 mm). Estimating E_c requires a good estimation of the bulk modulus, B, of the rubber, which is challenging to measure and varies significantly in the literature (1000–4200 MPa, Kelly & Konstantinidis (2011)). Three approaches were used to compute E_c of a single rubber layer:

1. Australian Standard AS 5100.4:2017: Using three different values of B (2000, 2500, and 3000 MPa) to calculate E_c, given its significant uncertainty in the literature, K_v = 4847, 5425, and 5895 MPa, respectively.
2. Kelly & Konstantinidis (2011): Using analytical diagrams for rectangular bearings (for B = 3000 MPa) to determine E_c, K_v was estimated at 6200 MN/m .
3. Coladant (1995) experimental data: Approximately extracting E_c ($\approx$ 1100 MPa) from an experimental curve (refer to Fig. V-2.12) led to K_v = 6540 MN/m.

5

The estimated range of K_v is 4847–6540 MN/m. Based on this, K_v = 6000 MN/m was assumed for each isolator in the blind prediction stage.

For the viscous damping coefficients C_h and C_v of the Kelvin-Voigt elements, a 7% damping ratio was adopted (Viallet et al., 2022), yielding C_h= 278 kN/m*s in the x and y directions and C_v= 4875 kN/m*s in the z direction, assuming a single-degree-of-freedom behavior for the nuclear island.

Blind prediction results

At this stage, blind prediction results from the two different models are presented: (a) a DRM model generating a three-component ground surface motion matching the provided RAN motion; and (b) a fixed-base model applying the three-component RAN motion directly at the base. Figure 5 compares the response spectra (5% damping) in the x, y, and z directions at EAU 001 (reactor building base), EAU 002 (internal structure of the reactor building), and EAU 003 (auxiliary building base) against the recorded data.

The recorded data indicate fundamental vibration modes at 1.54 Hz (x direction) and 1.7 Hz (y direction), along with higher-frequency modes for the reactor building. The DRM model underestimates both the fundamental modes and higher-frequency vibrations (> 4 Hz). Additionally, its predicted fundamental frequencies are slightly lower than those in Figure 4, likely due to SSI. The fixed-base model better approximates the fundamental peak in magnitude (though still underestimated) and frequency. However, it fails to consistently predict higher-frequency responses, sometimes overestimating and at other times underestimating the recorded data, making it less reliable for later calibration.
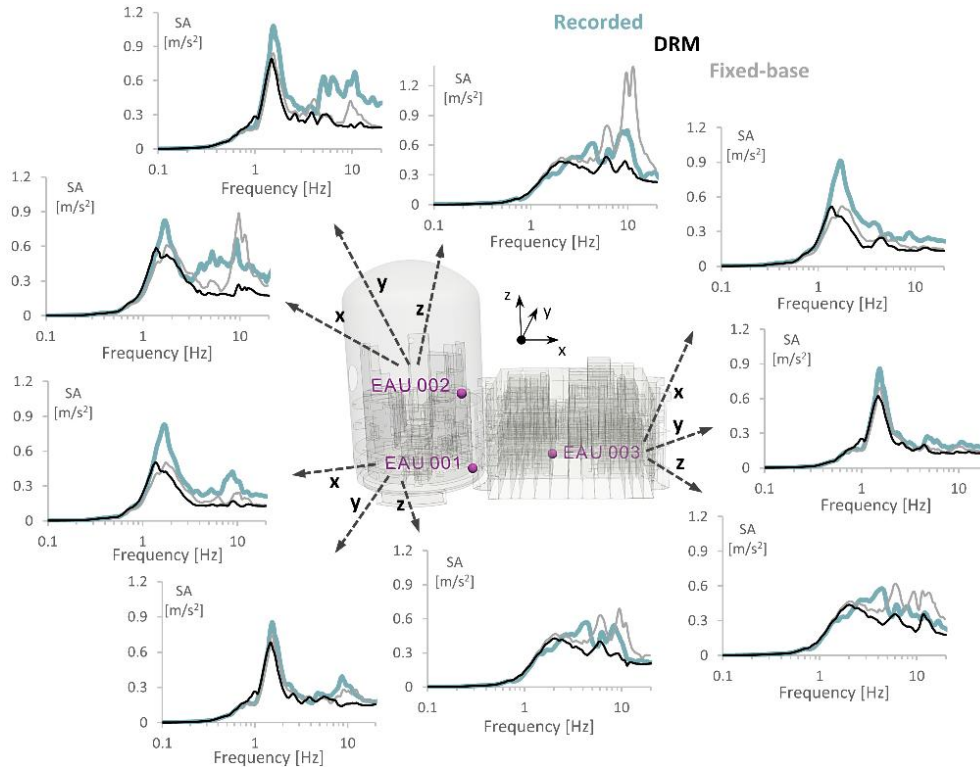

Figure 5. Horizontal (x and y) and vertical (z) acceleration response spectra at 5% damping for points EAU 001, 002, and 003. Comparison of the recorded data (petrol) with the two blind prediction models: the first DRM model targeting the free-field motion at the ground surface (black), and the fixed-base model excited at its base with the free-field motion (grey).

PART II – CALIBRATION OF DRM MODEL

Calibrated parameters

The DRM model is selected for calibration as it consistently underestimates the recorded data and accounts for the finite stiffness of the lower raft foundation and surrounding soil layers. The first parameter requiring calibration is the effective horizontal stiffness of the isolators. Figure 6a presents an example of horizontal force–shear displacement curves for two horizontal Kelvin-Voigt elements of the same isolator in the blind prediction stage. The results indicate different maximum shear displacements in the x (distortion ≈ 0.034) and y (distortion ≈ 0.045) directions, while the effective horizontal stiffness remains identical, as expected. However, laminated steel-neoprene bearings exhibit nonlinear behavior (Grant et al., 2004), meaning that an equivalent linear approach requires different effective horizontal stiffness values depending on the distortion level. Since the shear displacement in the x direction is smaller (closer to elastic response) than in the y direction, the isolators should exhibit higher stiffness in the x direction (Figure 6b).
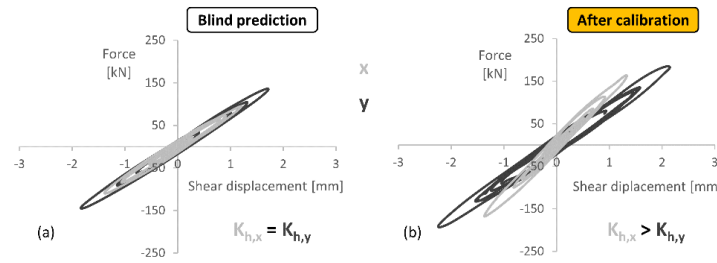

Figure 6. Typical horizontal force–shear displacement response of an isolator (Kelvin-Voigt elements) in the x and y directions: (a) during the blind prediction phase (same effective stiffness in both directions); and (b) after the calibration process (greater effective stiffness in the x direction).

By increasing the horizontal stiffness of the isolators in the x direction, spectral accelerations at the fundamental vibration mode were also increased (Figure 7). After calibration, final effective horizontal stiffness values were selected as $K_{h,x}$ = 30.5 MN/m and $K_{h,y}$ = 21.3 MN/m. Although the damping ratio of the isolators also affected the fundamental vibration mode, it was maintained at 7% in accordance with the literature and provided data.
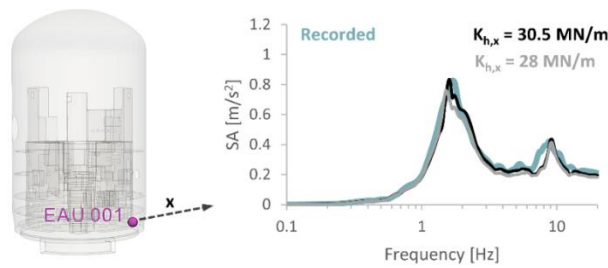

Figure 7. Influence of the horizontal stiffness $K_{h,x}$ on the acceleration response spectrum (5% damping) at point EAU 001 in the x direction. An increase in stiffness leads to higher spectral acceleration amplitudes at the lower frequency mode. The recorded data are included for reference.

Based on the fixed-base model's ability to capture higher-frequency vibration modes that were absent in the DRM model, it was considered reasonable to investigate the influence of soil stiffness on the response. This was further supported by the fact that the provided soil profile for the blind prediction phase (Figure 8b) corresponded to the RAN sensor location, which is not directly adjacent to the NPP, as shown in Figure 8a. Given the likelihood of soil improvement or stiffening due to adjacent NPP buildings, the
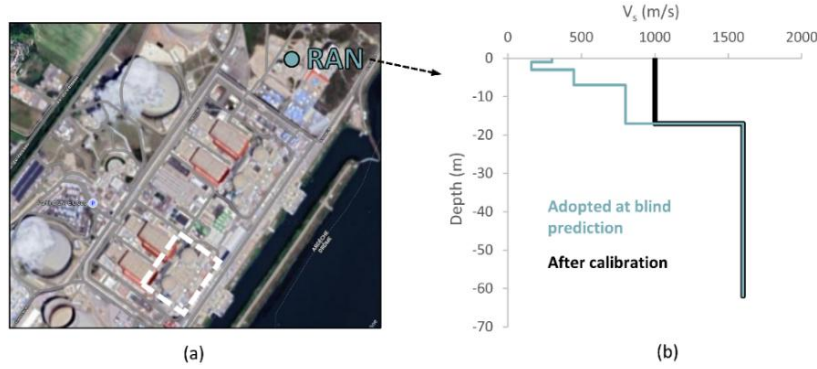
7

Figure 8. (a) Top view of the Cruas NPP site (sourced from Google Maps), showing the locations of the studied buildings (highlighted with a dashed rectangle) and the free-field RAN sensor. (b) Shear wave velocity profile used during the blind prediction phase (petrol) and the updated profile adopted after the calibration process (black).

shear wave velocity of the soil layers in the DRM model was progressively increased. This resulted in the emergence of higher-frequency vibration modes, as shown in Figure 9. Comparing response spectra of point EAU 002 in the x direction for three different soil profiles—original (light grey); V_S = 1000 m/s for the first four layers (black); and V_S = 2000 m/s for the first four layers (dark grey)—demonstrated that increasing soil stiffness leads to amplification of higher frequency vibration modes (aligning with the results of the fixed-base model). The final selected profile assumed V_S = 1000 m/s (Figure 8b).
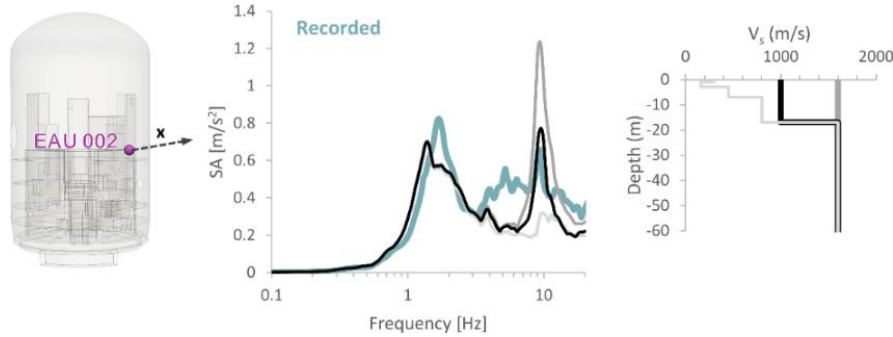

Figure 9. Influence of the shear wave velocity profile on the acceleration response spectrum (5% damping) at point EAU 002 in the x direction. An increase in soil stiffness leads to higher spectral acceleration amplitudes at the higher frequency mode. The recorded data are also plotted for reference.

The Rayleigh damping ratio of the structural components also influences the response amplitudes but was kept unchanged (i.e., 2%). Other parameters—including the vertical stiffness and damping of the isolators, the Rayleigh damping ratio of soil layers, and the stiffness of the perimeter wall and bonded contact elements—were examined but found to have negligible effects and are not discussed further.

Calibrated results

With the DRM model calibrated, Figure 10 shows the acceleration time history at point EAU 001 in the x direction, demonstrating remarkable agreement with the recorded data. The corresponding time-frequency diagrams, obtained using the Stockwell transform, further confirm this agreement. Figure 11 presents the response spectra diagrams (5% damping) for all three points in all three directions for the calibrated DRM model. The results indicate that the model successfully captures both the lower-frequency fundamental vibration modes in the x and y directions and the higher-frequency ones in the x, y, and z directions.
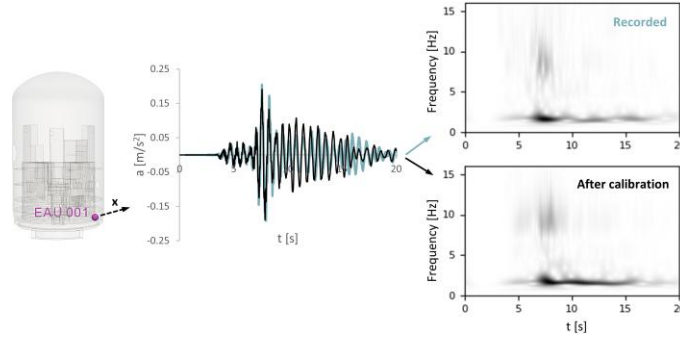
8

Figure 10. Comparison of the calibrated acceleration time history response at point EAU 001 in the x direction and its corresponding time-frequency diagram (black) with the recorded data (petrol).
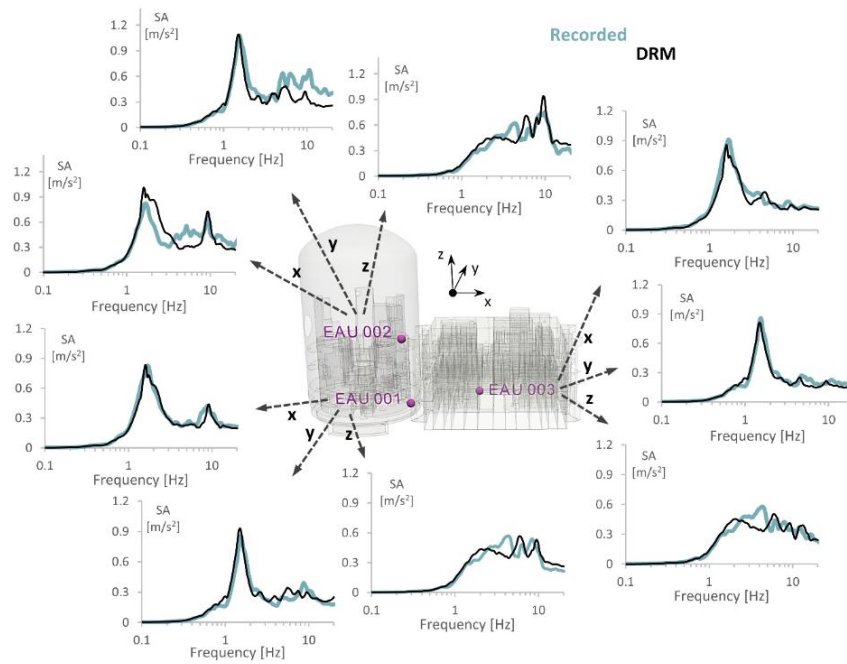

Figure 11. Horizontal (x and y) and vertical (z) acceleration response spectra at 5% damping at points EAU 001, 002, and 003. Comparison of the recorded data (petrol) with the updated first DRM model after the calibration process (black).

SUMMARY AND CONCLUSIONS

This study examines the seismic response of the base-isolated Cruas NPP during the Le-Teil earthquake using a fixed-base 3D FE model and a 3D DRM FE model, analyzed with the Real-ESSI software. The objective was to predict the seismic response at three sensor locations within the NPP—two in the reactor building and one in the auxiliary building—where the earthquake was recorded.

In the blind prediction phase, a DRM-based NPP model introduced vertically propagating S- and P-waves, reproducing the provided three-component free-field motion (RAN) at the ground surface. For comparison, a second simplified model, neglecting SSI effects, applied the same RAN motion directly at the base of a fixed-base NPP model. The nonlinear hysteretic shear behavior of the laminated steel-neoprene bearings was approximated using two horizontal springs and viscous dampers, initially assuming identical effective stiffness in both directions, targeting the provided eigenmodes and eigenfrequencies of the fixed-base NPP model. Between the two models, the fixed-base model provided overall the best approximation

9

of the recorded data. However, no general conclusion can be drawn because of possible inconsistency between the actual seismic input consisting of surface and inclined waves and the used approach assuming vertically incident waves. The DRM model, which accounts for the finite stiffness of the lower raft foundation and surrounding soil layers, was selected for calibration.

In the calibration phase, the DRM model was refined to better match the recorded data. It was found that assuming a single effective horizontal stiffness for the isolators was inadequate, as the isolators exhibited different distortions in the x and y directions. Consequently, two distinct stiffness values were introduced. While the fundamental vibration mode was primarily influenced by the isolators' horizontal stiffness (stiffer springs amplify spectral acceleration amplitudes), the higher-frequency modes were strongly affected by the assumed soil stiffness (stiffer soil profiles increase spectral acceleration amplitudes). A more realistically assumed soil profile, stiffer than initially provided, significantly improved the model's accuracy. After calibration, the DRM model successfully captured both the fundamental and higher-frequency vibration modes observed in the recorded data.

Despite achieving good agreement with the recorded data after calibration, further refinements are possible, including—but not limited to—the following:

(a) Implementing advanced isolator models to explicitly capture their nonlinear hysteretic shear behavior across all distortion levels;

(b) Replacing simplified stick models of NPP buildings with more detailed 3D representations;

(c) Accounting for the uncertainty of the model parameters, especially those related to soils;

(d) Developing a high-fidelity regional wave propagation model of the Le-Teil earthquake, including free-field sensors, to introduce more realistic seismic motions via DRM, incorporating all relevant seismic waves. A preliminary attempt was made during the first phase of the benchmark, but it is not included in this study.

REFERENCES

Ahrens, J., Geveci, B., & Law, C. (2005). *ParaView: An End-User Tool for Large Data Visualization*. Elsevier. https://www.paraview.org

Bielak, J., Loukakis, K., Hisada, Y., & Yoshimura, C. (2003). Domain reduction method for three-dimensional earthquake modeling in localized regions, part I: Theory. *Bulletin of the Seismological Society of America*, *93*(2), 817–824. https://doi.org/10.1785/0120010251

Clough, R. W. (1995). *Recent advances in earthquake engineering and structural dynamics* (V. E. Davidovici (ed.)). Editions Ouest-France.

Geuzaine, C., & Remacle, J.-F. (2009). Gmsh: A 3-D finite element mesh generator with built-in pre-and post-processing facilities. *International Journal for Numerical Methods in Engineering*, *79*(11), 1309–1331.

Grant, D. N., Fenves, G. L., & Whittaker, A. S. (2004). BIDIRECTIONAL MODELLING OF HIGH-DAMPING RUBBER BEARINGS. *Journal of Earthquake Engineering*, *8*(sup001), 161–185. https://doi.org/10.1080/13632460409350524

Jeremic, B., Jie, G., Cheng, Z., Tafazzoli, N., Tasiopoulou, P., Pisano, F., Abell, J., Watanabe, K., Feng, Y., Sinha, S. K., Behbehani, F., Yang, H., Wang, H., & Others. (2025). The Real ESSI Simulator System. In *University of California, Davis*. http://real-essi.us/

Kelly, J. M., & Konstantinidis, D. A. (2011). *Mechanics of Rubber Bearings for Seismic and Vibration Isolation*. Wiley. https://doi.org/10.1002/9781119971870

McKenna, F., Scott, M. H., & Fenves, G. L. (2010). Nonlinear Finite-Element Analysis Software Architecture Using Object Composition. *Journal of Computing in Civil Engineering*, *24*(1), 95–107. https://doi.org/10.1061/(ASCE)CP.1943-5487.0000002

Viallet, E., Berger, J., Traversa, P., El Haber, E., Hervé-Secourgeon, E., Hervé-Secourgeon, G., Zuchowski, L., & Dupuy, G. (2022). *2019-11-11 Le Teil Earthquake-The ultimate missing piece of experience feedback related to a Nuclear Power Plant built on seismic base isolation: A real earthquake.*